LEGIBILITY NOTICE

A major purpose of the Technical Information Center is to provide the broadest dissemination possible of information contained in DOE's Research and Development Reports to business, industry, the academic community, and federal, state and local governments.

Although a small portion of this report is not reproducible, it is being made available to expedite the availability of information on the research discussed herein.

LA-UR -87- 2807

LA-UR--87-2807

DE87 014764

TITLE SIMULATION OF THE LAYER-GROWTH DYNAMICS IN SILVER FILMS: DYNAMICS OF ADATOM CLUSTERS AND VACANCY CLUSTERS ON Ag(100)

AUTHOR(S) A. F. Voter

SUBMITTED TO 31st Annual Technical Symposium on Optical and Optoelectronic Applied Science and Engineering - The San Diego Meeting
San Diego, California
August 20-21, 1987

DISCLAIMER

Los Alamos Los Alamos National Laboratory
Los Alamos, New Mexico 87545

Simulation of the Layer-Growth Dynamics in Silver Films: Dynamics of Adatom and Vacancy Clusters on Ag(100)

Arthur F. Voter

Theoretical Division, MS J569, Los Alamos National Laboratory
Los Alamos, New Mexico 87545

ABSTRACT

Simulation results are presented for some dynamical processes occurring in the growth of (100) layers of silver. The overlayer dynamics are evolved using a recently developed method that, in the regime where surface diffusion consists of discrete hops, yields classically exact dynamics for an arbitrary interatomic potential. The time-scale limitations of direct molecular dynamics simulations are thus overcome. The Ag/Ag(100) system is modeled using a sophisticated form of interaction potential, similar to the embedded atom method, in which the energy is given by a sum of pairwise interactions plus a term for each atom that depends on the local atomic density. This type of potential includes the many-body terms necessary to describe a variety of atomic environments, such as the perfect fcc metal, free surfaces, vacancies, interstitials, and even the diatomic molecule, but with the computational scaling of a simple pair potential. The present study focuses on some of the dynamics in a single layer of silver: the diffusion and dissociation of clusters of adatoms and vacancies. Some interesting features are observed, including a nonmonotonic decrease in diffusion constant with increasing cluster size, and a roughly constant mean square distance a cluster migrates before dissociation (ejection of a monomer).

I. INTRODUCTION

The growth of crystals and thin films, because of their widespread technological importance,[1,2] has received considerable theoretical attention,[3] often in the form of atomistic computer simulations.[3-8] To make predictions about film growth, these simulations must model large systems over long time scales. To facilitate this, simplifying assumptions are made about the microscopic details of the growth process. Because some macroscopic properties of a system are relatively insensitive to the details of the underlying microscopic force laws and dynamics, a model system that is properly chosen and properly applied can yield quite useful results. For example, the simple solid on solid model[3] correctly predicts the roughening transition and other features of a growing crystal, even though the crystal packing is nonphysical, surface diffusion is omitted, and the interatomic forces are reduced to a single parameter. In more sophisticated simlations, commonly employed simplifications include restricting the film to two dimensions, the use of hard spheres or hard spheres with additive interactions.

As an alternative to the model system approach, one can attempt to simulate thin film growth while maintaining a connection to the true microscopic force laws. In other words, for an arbitrary interatomic potential (which can, in principle, be chosen to be fairly realistic for the system of interest) one follows the growth process using classical dynamics.

The most direct way to accomplish this is by integrating a classical trajectory involving a few hundred or thousand atoms representing the substrate plus thin film, while periodically introducing new

atoms to the system from the gas phase.[9] Since the system's evolution is governed by the proper force laws, the resulting features (columnar growth, formation of voids, etc.) are physically correct for the chosen interatomic potential. However, this direct molecular dynamics (MD) approach is currently limited to simulation of a few thousand atoms for approximately a nanosecond or less, due to the present speed of computers. With these restrictions, the most meaningful results are obtained by simulating close-packed surfaces (e.g., fcc(111), which have lower activation barriers for diffusion, at relatively high temperatures.

We have recently developed a different approach to this type of problem.[10] With certain restrictions, the method provides classically exact surface dynamics over long time scales. The method is designed to treat the overlayer dynamics for a submonolayer coverage of adsorbates on a perfect crystal face. As such, it is well suited for modeling Frank-van der Merwe (layer-by-layer) film growth. Ideally, one would like to treat film growth in the general case, with adsorption, desorption, three-dimensional clusters, voids, etc. In principle, this method can be extended to handle such processes (as discussed below), but it is currently in its infant stages. At the present time, this approach offers access to dynamical properties that cannot be calculated by direct MD, and, as such, the two methods are complimentary. Even though neither approach is capable of a full-scale simulation of general film growth, the results can be used to improve the parameterization of more macroscopic models, or to test assumptions in these models.

The study presented here is meant to be a demonstration of the feasibility of this new method for calculating dynamical properties important to film growth using a realistic interatomic potential. In particular, we examine the diffusion and dissociation of two-dimensional clusters of silver atoms on the Ag(100) surface. The silver interactions are provided by a state-of-the-art embedded-atom type of potential, described in Section 2. To the extent that this potential is realistic, the calculated dynamical properties should be appropriate for a (100) layer of a silver film that is thick enough to be unperturbed by the underlying substrate.

2. INTERATOMIC POTENTIAL FOR SILVER

Because the results of a molecular dynamics or Monte Carlo simulations are only as accurate as the underlying interatomic potential, there is a motivation to develop high-quality potentials. Daw and Baskes[11] have recently presented a new form of interatomic potential, known as the embedded atom method, in which the total energy of a homonuclear system of n atoms is written as

$$E_i = \frac{1}{2}\sum_{i\neq j}\phi(r_{ij}) + \sum_i F[\rho_i] \quad , \tag{2.1}$$

where

$$\rho_i = \sum_{j(\neq i)} \rho(r_{ij}) \tag{2.2}$$

Here, r_{ij} is the scalar distance between atoms i and j; $\phi(r)$ is the pairwise interaction term; $\rho(r)$ is a function that is roughly the electron density at a distance r from an atom; and $F[\rho]$ is the "embedding function." This type of potential is discussed in detail elsewhere[11-13] and has been quite successful in providing a reasonably quantitative description of metallic systems in a variety of simulations.[14] We briefly discuss here some of the key features of this form of potential, and how we have chosen to parameterize $\phi(r)$, $\rho(r)$ and $F(\rho)$ for Ag.

If Eq. (2.1) is truncated after the first sum, a simple pair potential results. Such a potential has the virtue of computational simplicity and ease of parameterization, but suffers from some defects. For example, the vacancy formation energy (ΔE_{vac}) is equal to the cohesive energy (E_{coh}), and the elastic constants c_{12} and c_{44} are also equal, while neither of these equalities holds for real metal crystals. In a Lennard-Jones pairwise description of silver, the melting point is ~2.8 times to high.[15] The simple pair potential can be improved by introducing a volume dependence, i.e., a pair potential is derived that is appropriate for a particular density, or volume, of the system.[16] The motivation for this arises from viewing the metal crystal as ions immersed in a background electron gas.[17-19] The energy will depend strongly on the density of the electron gas and, hence, the volume of the system. While this modification to the pair potential corrects the three problems mentioned above,

it introduces the restriction that major defects such as a free surface cannot be treated, since the system cannot be characterized by a constant volume.

The embedded atom method allows a solution to this problem. In Eq. (2.1), the pair potential is augmented by a sum of embedding functions which, in effect, provide a local volume contribution to the energy for each atom. This is because ρ_i acts as a sensor for the crowding of atoms about atom i. Hence, with this form of potential, systems with a wide variation in density can be treated. The embedding function, F, provides a many-body contribution to the energy (assuming F is not purely linear), but the computational work involved in evaluating the energy and derivatives from Eq. (2.1) scales the same as a simple pair potential. However, there is no implicit angular dependence in Eq. (2.1), so it is inappropriate for systems with strongly directional bonding.

We now briefly describe the parameterization used in the present study for fcc silver. The details of both the fitting procedure and the parameterization philosophy can be found elsewhere.[21,22] The pair potential is taken to be a Morse potential,

$$\phi(r) = D_M\{1 - \exp[-\alpha_M(r-R_M)]\}^2 , \qquad (2.3)$$

with three adjustable parameters, R_M, D_M, and α_M. The density function is defined as

$$\rho(r) = r^6[e^{-\beta r} + 512e^{-2\beta r}] , \qquad (2.4)$$

which is designed to roughly mimic the electron density of a transition metal atom,[23] with adjustable parameter B. Both $\phi(r)$ and $\rho(r)$ are modified to go smoothly to zero at a cutoff distance, r_{cut}, which is also an adjustable parameter. Following Foiles et al.,[14,24] for each choice of these five parameters, $F(\rho)$ is defined by specifying that the total energy [from Eq. (2.1)] of an fcc crystal follow the form

$$E(a^*) = -E_{coh}(1 + a^*)e^{-a^*} \qquad (2.5)$$

where a^* is a reduced distance variable given by

$$a^* = (a/a_0 - 1)/(E_{coh}/9B\Omega)^{1/2} , \qquad (2.6)$$

Here a is the lattice constant, a_o is the equilibrium lattice constant, B is the bulk modulus, E_{coh} is the cohesive energy of the fcc crystal, and Ω is the atomic volume. The use of Eq. (5) to define $F(\rho)$ is motivated by the finding of Rose et al.[25] that results of density functional calculations on solids show a behavior similar to Eq. (5). This approach ensures reasonable behavior over a wide range of atomic densities, and leads to a potential that gives exact agreement with the experimental lattice constant, cohesive energy and bulk modulus.

The five parameters (R_M, D_M, α_M, β and r_{cut}) are optimized using a simplex search procedure,[26] by minimizing the root-mean-square deviation (χ_{rms}) between the calculated and experimental values for the three cubic elastic constants (c_{11},c_{12}, and c_{44}), the vacancy formation energy (ΔE_{vac}), and the bond length (R_e) and bond strength (D_e) of the diatomic molecule Ag_2. The bcc and hcp crystal structures are also required to be higher in energy than fcc. The resulting fit, shown in Table I, has $\chi_{rms} = 0.15\%$, and the parameter values are $D_M = 0.672$ eV, $R_M = 2.570$ Å, $\alpha_M = 1.826$ Å^{-1}, $\beta = 3.906$ Å^{-1}, and $r_{cut} = 5.542$ Å.

TABLE I. - Experimental properties used in fit for Ag potential, along with the calculated values from the best fit. The values for a_o, E_{coh}, and B are fit exactly, due to the way $F(\rho)$ is obtained.

	experiment	calculated
a_0 (Å)	4.09[a]	
E_{coh} (eV)	2.85[b]	
B (10^{12} erg cm^{-3})	1.04[c]	
c_{11} (10^{12}erg cm^{-3})	1.24[c]	1.24
c_{12} (10^{12}erg cm^{-3})	0.934[c]	0.935
c_{44} (10^{12}erg cm^{-3})	0.461[c]	0.461
ΔE_{vac} (eV)	1.1[d]	1.10
D_e (eV)	1.66[e]	1.66
R_e (Å)	(2.5)[f]	2.504

[a]Reference 27
[b]Reference 28
[c]Reference 29
[d]Reference 30
[e]Reference 31
[f]Reference 32

3. OVERLAYER DYNAMICS METHOD

We describe here the method used to follow the dynamics of an evolving pattern of adsorbed atoms. This recently developed method has been presented in detail elsewhere.[10] The key feature of this approach is that, for a certain class of systems, it can provide classically exact, course-grained dynamics for the evolution of an overlayer pattern, starting from an arbitrary interatomic potential. The method is restricted to systems in which the adsorbed species bind in registry with the surface, and to temperatures below the melting point of the surface (since a melted surface would not have well-defined binding sites). In the present work, we further impose the condition that the temperature be low enough that transition state theory is valid, as discussed below. Since the focus here is on Ag adatoms on the Ag(100) surface, the method will be described as it applies to that type of system.

3.1. Single-atom diffusion

Consider a single adatom on an fcc(100) face. For silver the stable binding site is in the fourfold hollow, and diffusive jumps to adjacent binding sites take place via the twofold saddle point which separate these fourfold sites, as shown in Fig. 1. Given a particular interatomic potential, which defines the adatom-substrate and substrate-substrate interactions, the classical thermal rate constant for escape from this binding site can be rigorously computed using transition state theory[33,34] (TST) combined with dynamical corrections. In the TST approximation, the rate constant for transfer of a system between two states is given by the thermal flux through a dividing surface that separates the states. (For the fcc(100) surface, a good choice for the TST dividing surface is a square whose corners are defined by the four atoms holding the adatom. When the adatom coordinates, projected onto the plane parallel to the surface, coincide with this square, the system is at the TST surface.) The TST rate constant is thus an equilibrium property of the system and can be rigorously computed using Metropolis Monte Carlo methods, as described elsewhere.[35,36]

Even if the TST surface is positioned such that the transition flux is minimized, TST does not give the true dynamical rate constant, because each crossing of the TST dividing surface does not necessarily correspond to a reactive state-change event. For example, a system passing from state A to state B may jiggle around in the region of the dividing surface, recrossing it many times before thermalizing in state B. Moreover, for a system consisting of surface binding sites, an energized adatom may make multiple hops, thermalizing in a binding site many sites away from where it started to hop. The effects of these "correlated dynamical events" can be accounted for in a rigorous fashion (regardless of the position of the TST surface) using a many-state dynamical corrections method,[37] which is an extension of a two-state formalism presented by Chandler.[38] This formalism is strictly applicable when the time duration of the correlated dynamical events (τ_{corr}) is much shorter than the average time between reactive transitions (τ_{rxn}),

$$\tau_{corr} << \tau_{rxn} \tag{3.1}$$

The method is implemented computationally by initiating a statistical sampling of classical trajectories at the TST dividing surface and integrating them until the correlated events cease. The result is that the true rate constant between state i and any other state (j) of

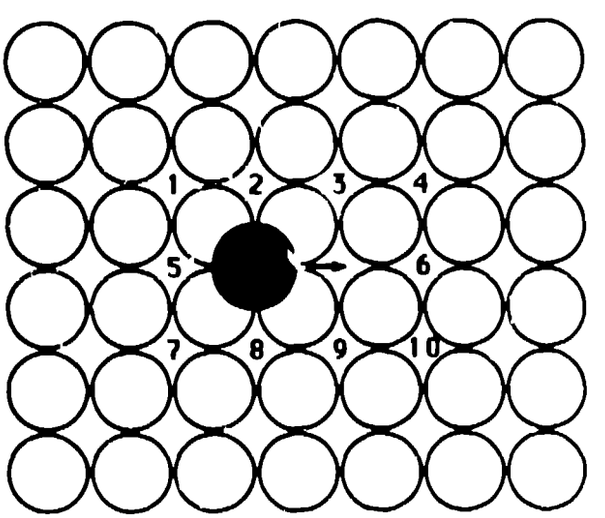

Fig. 1. Top layer of the substrate pad used to compute the rate constants for Ag/Ag(100). The ten binding sites making up the local environment are shown. All the 43 atoms shown (plus between zero and ten environment adatoms) are allowed to relax in each of the 2^{10} harmonic TST computations

the system can be written as

$$k_{i\to j} = k_{i\to}^{TST}\, f_d(i\to j)\ , \qquad (3.2)$$

where $k_{i\to}^{TST}$ is the TST rate of escape through the dividing surface enclosing state i, and $f_d(i\to j)$ is the dynamical correction factor obtained from an analysis of the half-trajectories that originated at the boundary to state i. The total (diffusive) escape rate from state i is given by

$$k_{i\to} = \sum_{j(\neq i)} k_{i\to}^{TST}\, f_d(i\to j)\ . \qquad (3.3)$$

The surface diffusion process provides a good example of the motivation for expressing the rate constant using TST with dynamical corrections. Using Eq. (3.1), the diffusion constant for a single adatom on a two-dimensional periodic surface becomes

$$D = \frac{1}{4}\, k_{i\to}^{TST} \sum_{j(\neq i)} f_d(i\to j)\ \ell_{ij}^2\ . \qquad (3.4)$$

where ℓ_{ij} is the distance between binding sites i and j. In the temperature regime where Eq. (3.1) holds, it is relatively straightforward to compute D from Eq. (3.4). Alternatively, D can be computed from one long classical trajectory, from the time derivative of the mean squared displacement of the adatom position. However, this is completely unfeasible at low temperatures, due to the long time between diffusive hops of the adatom. In contrast, the trajectories in the dynamical corrections method are only integrated for a short time, since they *start* at the TST dividing surface, i.e., in the middle of a hop, and are only run until the hop is completed.

In previous studies on Lennard-Jones systems,[37] we have found that at low to moderate temperatures the dynamical corrections are usually negligible, affecting the diffusion constant by only a few percent (compared to the TST approximation). Moreover, we have shown[10] that reasonably accurate TST rates can be calculated using a harmonic approximation, given by

$$k^{HTST} = \nu_0 \exp[(E_{saddle}-E_{min})/k_BT] \qquad (3.5)$$

where ν_0 is a harmonic frequency, k_B is the Boltzmann constant, T is the temperature, and E_{min} and E_{saddle} are the energies at the adatom minimum and the saddle point between two binding sites, respectively. These energies are found by performing a Newton-Raphson search for stationary points in the hyperspace defined by the Cartesian coordinates of all moving atoms. The frequency factor ν_0 is computed from the second derivatives of the energy at the minimum and the saddle point.[10]

For computational convenience, we make use of this harmonic TST approximation in the present work.

3.2. Multiple, interacting adatoms

Now consider a distribution of interacting, adsorbed adatoms. The escape rate constant for any adatom in this overlayer will depend on its environment of nearly adatoms. Using the methods described above, this rate can be calculated for a hop in a particular direction. If these hopping rate constants are known for all atoms in the system at all times, then by using the appropriate thermodynamic statistics, the overlayer pattern can be dynamically evolved. If the rate constants are classically exact, then the overlayer dynamics will also be classically exact, in a course-grained sense; one can only ask about dynamical behavior for time scales much longer than the time between adatom hops. The spirit of the overlayer dynamics method employed here is to precalculate all possible rate constants that might be needed and store them in a catalog that is referenced during the dynamical simulation. More specifically, we define a ten-atom environment surrounding an adatom and the empty binding site in which it will land upon hopping to the right, as shown in Fig. 1. Since each of the ten sites can be empty or occupied, there are 2^{10}=1024 rate constants to be calculated (some of which will be equivalent by symmetry). Computation of this rate catalog is carried out in an automated fashion using the harmonic TST approximation described above. Once the catalog has been generated, the dynamics of an arbitrary overlayer pattern of N atoms is evolved as follows:

(i) Use the catalog to look up the appropriate value of the directional escape rate, k_{esc}, for each of the

$4N_{atom}$ possible hops (each atom has four possible hop directions). For hops that are blocked by an adatom in the adjacent binding site, $k_{esc}=0$.

(ii) Increment the clock by

$$\Delta t_{hop} = \left[\sum_{i=1}^{4N_{atom}} k_{esc}(i) \right]^{-1} \qquad (3.6)$$

which is the time, on average, before *some* atom in the overlayer makes a hop.

(iii) Randomly select one of the $4N_{atom}$ possible hops, weighting the probability of selection of each hop by k_{esc}.

(iv) Go to (i).

As stated above, for the chosen interatomic potential, this procedure leads to classically exact, course-grained dynamics for the overlayer, including the motion and response of the substrate, within the assumption that the rate catalog is exact. The two approximations in the cataloged rates are of a controlled nature: they can be tested, improved and, in principle, eliminated. The first of these approximations lies in the method used to compute the rate constants; harmonic TST is employed, and the dynamical corrections are omitted. This approximation is good at low temperatures. The second approximation arises from truncating the environment at ten atoms, since the true rates will clearly depend on more distant adatoms. The motivation for this lies in the fact that 2^m rates must be calculated for an m-site environment. The effect of more distant adatoms can be tested, as discussed in the next section. In the present study, the approximation having the greatest effect on comparison to experiment is probably the silver interatomic potential described in Section II, even though it is at the present state of the art.

All dynamical properties that can be calculated with standard lattice-gas methods, such as tracer and chemical diffusion constants, autocorrelation functions of adsorbate density fluctuations and island nucleation rates, can also be computed using the present method. The method can be used with any interatomic potential, as long as the adsorbate binds in registry and Eq. (3.1) is satisfied. This approach, for the first time, provides a connection between stochastic lattice-gas techniques and the interatomic potential.

To conclude this section, we briefly discuss extensions of the method necessary to treat the more general case of thin film growth. None of these extensions are employed in the present work.

Treating desorption with this method is straightforward. The rate constant catalog is augmented to include rate constants for desorption of an adatom, so that during the simulation, each adatom has a possibility of desorbing or diffusing that depends on its environment. The TST desorption rate constant for a given environment is computed from the flux through a plane, parallel to the surface, that caps the top of the binding site. Dynamical corrections, if desired, can be computed by initiating trajectories from this plane and following them for a time τ_{corr}.

Treating adsorption, as is necessary to model film growth, is also straightforward. Dynamical corrections are computed in the same way as for desorption, and the *same* set of trajectories can even be used if the impinging atoms are assumed to be in thermal equilibrium with the growing film (i.e., the dynamical correction factor for desorption is the same as the thermal sticking coefficient if the TST surface is far enough from the surface). During the simulation, new atoms are introduced to the system at a rate dictated by the temperature and pressure of the vapor phase and the dynamical correction factors give the relative probabilities of sticking, sticking in a nearly binding site, or completely bouncing off the surface. Note that if a nonthermal distribution of incoming atoms is assumed (e.g., for molecular beam epitaxy), then the dynamical correction factors must be computed for that distribution, and will be different than the desorption correction factors.

The simulation of general film growth requires that the surface be allowed to have terraces, vacancies, etc., rather than being defect free as assumed above. In principle, the rate catalog can be extended to include jumps up or down steps, jumps in the presence of a surface or bulk vacancy, and so forth. In practice, this increases the number of environment sites (m) substantially, so that calculating 2^m rate constants

becomes unfeasible. However, by judiciously choosing the environment patterns that are important to include for a particular case or type of process, it may be possible to perform this type of simulation.

4. Ag/Ag(100) CLUSTER DYNAMICS

In this section we discuss the simulation of the diffusion of two-dimensional clusters of adatoms and vacancies on Ag(100). There have been very few previous investigations of cluster motion (for a review, see Ref. 39), and until recently,[10] little was known about the motion of clusters larger than a few atoms. Understanding their dynamical behavior is useful, as the coalescence, diffusion and dissociation of clusters certainly play a role in layer-by-layer film or crystal growth, and in mass transport diffusion.

4.1 Calculational details

The Ag substrate used in the TST rate calculations was a four-layer block of atoms with 42 atoms per layer as shown in Fig. 1. Periodic boundary conditions were employed in the two directions parallel to the surface. For each harmonic TST calculation, the primary adatom, along with between zero and ten environment adatoms, were placed on top of this block, and these adatoms plus all of the first layer adatoms were allowed to move in the Newton-Raphson search. The layer size and block depth were made large enough to eliminate any boundary effects on the moving atoms. Generation of the rate catalog was automated as described previously.[10] For each of the 1024 environment patterns, a preexponential factor (ν) and an activation barrier ($E_A = E_{saddle} - E_{min}$) were stored, so that, using Eq. (3.5), the catalog could be employed to drive dynamics at any temperature (though the rates become more approximate at higher temperatures). Unless otherwise noted, calculations reported here were performed at T= 500K.

The effect of allowing relaxation of more than one substrate layer was tested by computing TST activation barriers for a single adatom. The barrier heights, expressed in kcal/mol, were found to be 11.68, 11.27, 11.18, 11.16 and 11.16, respectively, for relaxation of zero through six layers. Thus, as found previously,[35] accurate TST barrier heights for the fcc(100) surface can be obtained with only one layer relaxed.

The effect of the truncation of the catalog at ten binding sites was examined by generating a rate catalog for the 13-site environment shown in Fig. 2. This catalog includes six representative sites from the second shell (A-F), along with the seven sites from the first shell (1,2,3,5,7,8,9) thought to most strongly interact with the outer six. For each of the 4096 environment patterns, E_{min} and E_{saddle} were computed, along with E_∞, the energy with the primary adatom removed from the system. The energy required to desorb the primary adatom from the minimum is

$$E_1 = E_\infty - E_{min} , \tag{4.1}$$

the energy to desorb the adatom from the saddle point is

$$E_2 = E_\infty - E_{saddle} , \tag{4.2}$$

and the activation energy can be written as

$$E_A = E_1 - E_2 . \tag{4.3}$$

The analysis of these energies is shown in Table 2. For each of the 13 sites, the effect (ΔE) of removing the adatom from that site was determined. For example, removing the adatom from site A can raise E_A by as much as 0.76 kcal/mol, or lower it by 0.07 kcal/mol. These values are determined by scanning the 2048 pairs of patterns (patterns in a pair are the same except for the occupation of site A), and finding the largest deviations in E_A. The magnitude of ΔE gives an indication of the effect a particular site has on the catalog energies, while the difference between ΔE_{max} and ΔE_{min} is a measure of the nonadditivity of the interactions. Note that the nonaddivity effects on E_A can be greater than 5 kcal/mol (see site 3). Of the sites omitted from the present work (A-F), site F appears to be most important, with ΔE_A ranging from -0.98 kcal/mol to 0.18 kcal/mol.

From an examination of ΔE_1, and ΔE_2, it is clear that different sites are important for the accuracy of E_1 than for E_2. For example, the sites having more than

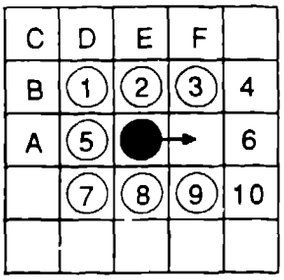

Fig. 2. The 13 sites used in computing a rate catalog to test the effect of environment size (see Table 2). To simplify the comparison with the 10-site environment used in the present work, the numbering of the first ten sites is maintained, even though only the circled sites were included in the catalog (4,6, and 10 were omitted). Sites A-F are outside the environment of the 10-site catalog used in the present dynamical calculations.

Table 2. Analysis of the 13 sites in Fig. 2, according to how much the desorption energy and activation energy of the primary adatom changes when the site atom is removed. ΔE is the change in desorption energy (kcal) upon site removal; ΔE_1 refers to desorption of the primary adatom from the minimum; ΔE_2 refers to the desorption of the primary adatom from the saddle point; ΔE_A refers to the activation energy of the primary adatom; min = lowest ΔE found in list of all configurations; max = highest ΔE found in list of all configurations.

	ΔE_1		ΔE_2		ΔE_2	
site	min	max	min	max	min	max
1	-0.85	-0.02	-0.32	0.87	-1.56	-0.07
2	-7.24	-5.17	-7.39	-2.05	-3.99	0.55
3	-0.88	-0.31	-7.98	-2.49	1.74	7.38
5	-7.25	-5.40	-1.79	-0.18	-6.82	-4.37
7	-0.91	-0.07	-0.32	0.72	-1.44	-0.16
8	-7.31	-5.76	-7.45	-2.40	-3.95	0.63
9	-0.95	-0.42	-7.85	-2.86	2.06	7.30
A	-0.08	0.76	-0.14	0.27	-0.07	0.76
B	-0.05	0.32	-0.14	0.09	-0.07	0.30
C	-0.06	0.09	-0.11	0.03	-0.05	0.12
D	-0.05	0.38	-0.16	0.39	-0.26	0.19
E	-0.09	0.76	-0.15	1.22	-0.56	0.50
F	-0.03	0.33	-0.10	1.17	-0.98	0.18

-0.5 kcal/mol effect on E_1 are 1,2,3,5,7,8,9,A, and E, whereas the sites having more than 0.5 kcal/mol effect on E_2 are 1,2,3,5,7,8,9,E, and F. Thus, using the 11-atom environment shown in Fig. 3a to compute a catalog of E_{min} values and the 14-atom environment in Fig. 3b to compute a catalog of E_{saddle} values would lead to a combined catalog converged such that any site added to the environment would affect E_A by less than 0.5 kcal/mol. (The union of these two environments has 15 sites, which would require 2×2^{15} calculations, rather than $2^{11} + 2^{14}$ calculations.)

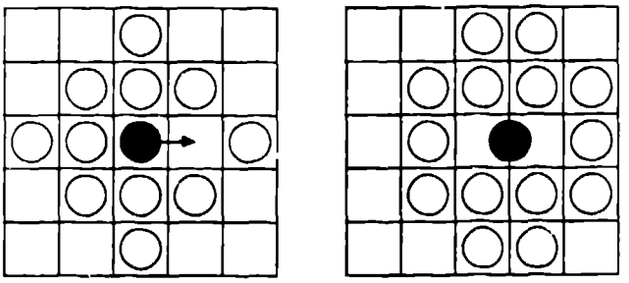

Fig. 3. Environments deduced from Table 2, for computation of a catalog good to better than 0.5 kcal/mol (see text). a) 11-site environment for computing E_{min}; b) 14-site environment for computing E_{saddle}.

To improve the accuracy of the vacancy cluster simulations presented here, a second 10-site catalog was computed, in which all the binding sites outside of the 10-atom environment were occupied with Ag adatoms. Comparing this catalog to the first 10-site catalog shows a maximum deviation in E_A of 2.96 kcal/mol, a value that is in line with the findings above (989/1024 cases differed by less than 2 kcal/mol, and 807/1024 cases differed by less than 1 kcal/mol). The indices in this catalog were then transformed using a left-right reflection with occupation inversion,

$$
\begin{aligned}
1 &\rightarrow \bar{4} \\
2 &\rightarrow \bar{3} \\
3 &\rightarrow \bar{2} \\
4 &\rightarrow \bar{1} \\
5 &\rightarrow \bar{6} \\
6 &\rightarrow \bar{5} \\
7 &\rightarrow \overline{10}
\end{aligned}
$$

$$8 \rightarrow \overline{9}$$
$$9 \rightarrow \overline{8}$$
$$10 \rightarrow \overline{7}$$

to make the rates appropriate for a vacancy hop to the right (i.e., an adatom hop to the left). Using this special catalog, vacancy dynamics were evolved in exactly the same way as adatom dynamics.

The cluster diffusion constants were computed using an independent dynamical simulation for each cluster size. Simulations were performed on a square grid using periodic boundary conditions, with the grid size chosen to prevent interaction between the cluster and its periodic image. The following describes the procedure for one simulation.

The initial cluster configuration of n atoms was generated by placing atoms at random on the grid, rejecting any placement that broke the connectivity of the cluster. Two atoms are considered "connected" if they are first or second nearest neighbors (i.e., an adatom can be directly connected to up to 8 other atoms). This cluster configuration was then evolved in time, using the procedure described in Section 3, with the restriction that if a chosen hop broke the cluster connectivity, that hop was rejected (and the clock was not incremented). This nonphysical restriction was imposed so that a diffusion constant could be computed for a well-defined cluster. An alternative approach would be to compute a diffusion constant from the motion of clusters that have not yet dissociated. These two approaches become equivalent at very low temperature[39,40] (probably lower than 500K). After a suitable warmup period, the diffusion constant was computed from the time derivative of the mean-squared displacement of the cluster center of mass,

$$D_n = \lim_{t\to\infty} \frac{1}{4}\frac{d}{dt} < \Delta R^2_{cm}(t) > \qquad (4.4)$$

by examining equal-time snapshots taken from a long trajectory. Typical trajectories were run for millions of steps, corresponding to tens of milliseconds. The mean squared displacement of a ten-atom cluster is shown in Fig. 4.

4.2 Results and discussion

To gain a qualitative understanding of the overlayer dynamics, it is instructive to examine the rate constants as a function of environment pattern. Figure 5 shows some representative activation barriers from the adatom rate catalog and from the vacancy rate catalog. The barrier to diffusion for a single adatom is 11.3 kcal/mol. In principle, this activation energy can be measured experimentally using field ion microscopy,[41] but to our knowledge, no Ag/Ag(100) measurements have been performed. The diffusion barrier for a vacancy is 10.7 kcal, so single vacancies are somewhat more mobile than single adatoms. When the energy of formation from a kink site is taken into account, the predicted mass transport diffusion barrier is 26.1 kcal for an adatom and 22.6 kcal for a vacancy. Thus, this potential predicts that vacancy monomer diffusion dominates adatom monomer diffusion in mass transport.

The barrier for an adatom to jump away from a nearest-neighbor atom is 17.8 kcal/mol, 6.5 kcal greater than free migration, indicating a strong tendency for the silver adatoms to cluster, as expected. In contrast, the barrier for separating two nearest-neighbor vacancies is only 1 kcal/mol higher than free migration of a vacancy. In fact, the vacancy dimer is more likely to dissociate (Fig. 5b) than to make a

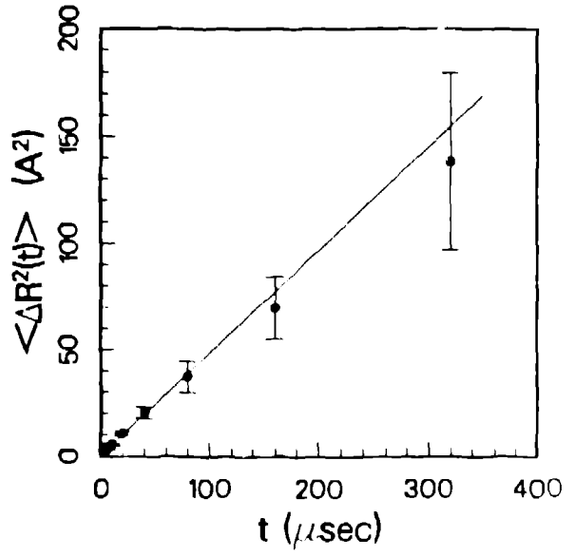

Fig. 4. Mean squared displacement of a 10-atom Ag cluster at T=500K.

diffusive step (Fig. 5c). For both the adatoms and the vacancies, the barrier for breaking out of the corner (Fig. 5d) or side (Fig. 5e) of a block is substantially larger than free monomers migration.

Figure 5f shows that an adatom can move easily along the edge of a perfect block, with a barrier of only 5.9 kcal/mol. The barrier for liberating an edge runner from a kink site on a cluster edge is 11.6 kcal/mol (Fig. 5g). At low temperature, where clusters tend to form tightly packed blocks, edge running can dominate the dynamics. This makes cluster diffusion simulation difficult, since edge running alone will not allow a cluster to diffuse. For vacancy clusters, this edge running has a barrier of 11.0 kcal, which will not dominate the dynamics. The vacancy edge-running that *does* occur is that of an edge-vacancy in the vacancy cluster (i.e., an adatom), but this adatom gets trapped at the corners, and thus does not so greatly dominate the dynamics.

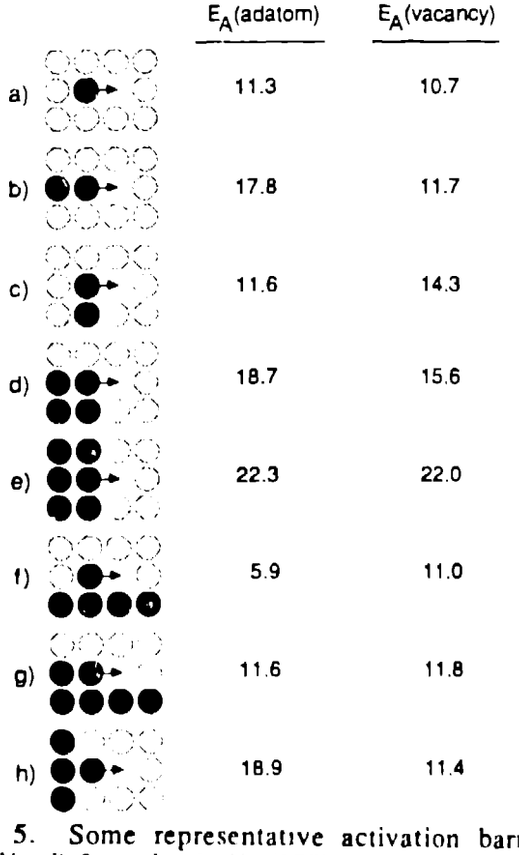

Fig. 5. Some representative activation barriers (kcal/mol) from the Ag/Ag(100) rate catalogs. Note that by particle-hole symmetry, the barriers for the adatom and the vacancy should be the same for (e) and also for (f). They differ due to the way the catalogs were generated.

Vacancy clusters also differ from adatom clusters in their greater propensity toward dissociation, as shown in Fig. 5h. Cluster dissociation rates at T=500K, estimated from the number of dissociating steps that were rejected during the run (this is not a rigorous dissociation rate), were ~10^3 times faster for the vacancy clusters when compared to adatom clusters of the same size.

Figure 6 shows the diffusion constants for clusters up to n=100 at T=500K. As expected, monomers (n=1) diffuse the fastest, but D_n does not decrease monotonically with increasing cluster size. This is because clusters that can form stable blocks (e.g., n=4,6,8) diffuse more slowly due to the long time required to break out of a perfect block structure (see Figs. 5d and 5e). Thus, for example, an n=4 cluster should have an activation barrier of 18.7 kcal/mol. In contrast, an n=5 cluster can diffuse with a maximum barrier of 12.8 kcal/mol, by following the sequence shown in Fig. 7. These values are in agreement with diffusional activation energies for n=4 and n=5 clusters obtained from Arrhenius plots. Both the adatom clusters and the vacancy clusters show this stable-block effect.

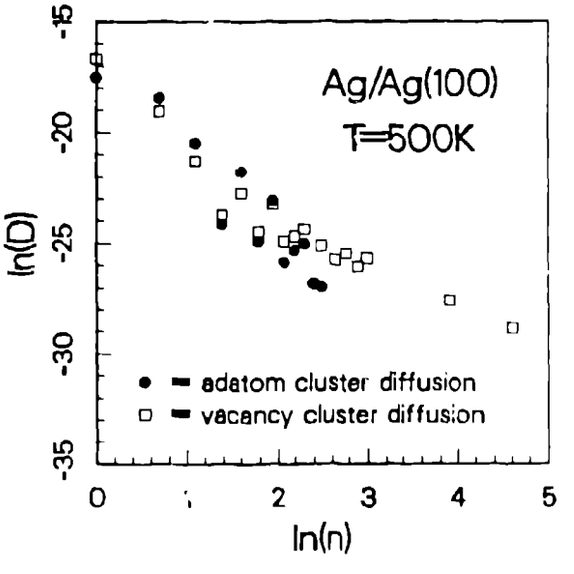

Fig. 6. Cluster diffusion constants (cm^2/sec) for Ag or Ag vacancies on Ag(100).

As in the previous study of Lennard-Jones clusters,[10] the dominant diffusion mechanism for large Ag clusters is found to be edge motion. To actually move the cluster, an adatom must climb onto a fresh edge from a kink site, surmounting a barrier of 19.2 kcal/mol, as shown in Fig. 8. This is in excellent agreement with the activation energy (19±2 kcal/mol) obtained from an Arrhenius plot of the diffusion of a 100-atom Ag cluster between T=600K and T=300K. Figure 9 shows successive snapshots of an n=100 adatom cluster and an n=100 vacancy cluster. The overall diffusion rates are seen to be roughly comparable. The 25-configuration sequence (5 msec) represents 1/40 of the total trajectory used to compute D_{100} for the vacancy cluster. In the adatom cluster, nonproductive edge running results in three times as many steps per unit time than for the vacancy cluster, making computation of a diffusion constant more difficult.

As mentioned above, the cluster lifetime (before dissociation) can be estimated by dividing the total trajectory time by the number of cluster-dissociating steps that were rejected during the run. This is not a rigorous calculation, but is a good approximation if many more steps are accepted than rejected (not always the case in the present work). Knowing this dissociation lifetime (τ_n) and the diffusion constant, the root mean square distance that a cluster will diffuse before dissociation can be estimated by

$$d_n = [4D_n\tau_n]^{1/2} \quad . \tag{4.5}$$

It is interesting to note that for adatom clusters d_n lies between 1Å and 10 Å for a large range of cluster sizes (up to n=40) and temperature (d_n decreases slowly as n increases and as T increases). For vacancy clusters the same effect is observed, but with d_n about ten times smaller. (Actual values for d_n are not given here due to

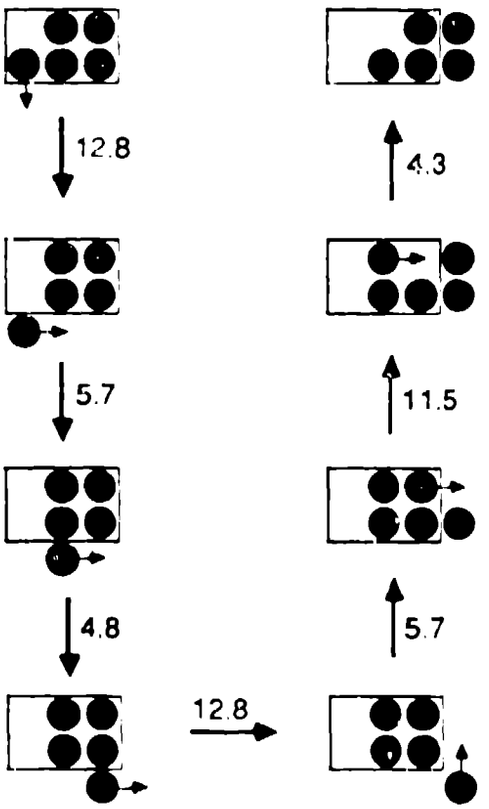

Fig. 7. Diffusion pathway for n=5 adatom cluster, in which the cluster is replicated one binding site to the right after 7 moves. The numbers are activation barriers in kcal/mol. The maximum barrier is 12.8 kcal/mol.

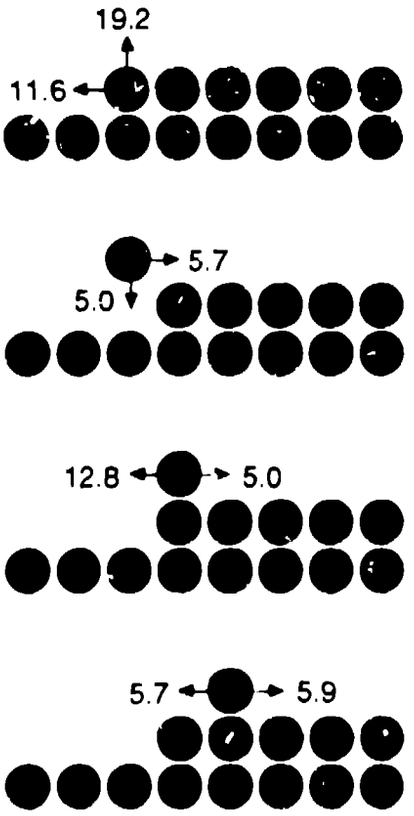

Fig. 8. Mechanism for an adatom to climb onto a fresh edge from a kink site. The maximum barrier in this process is 19.2 kcal/mol, in agreement with the Arrhenius activation energy for diffusion of a 100-atom Ag cluster.

the uncertainty in τ_n.) Under the right thermodynamic conditions, cluster diffusion may contribute significantly to mass transport, but these small values for d_n imply that the transport will *not* be via clusters moving long distances intact. Rather, a picture emerges in which slowly moving clusters are in equilibrium with rapidly moving monomers. A cluster captures any adatom that comes too close, but then ejects a monomer after it has diffused just a few angstroms (or a few tenths of an angstrom in the case of vacancy clusters). Thus, a cluster that has migrated a long distance (e.g. hundreds of angstroms), probably consists mostly of different atoms than when it started.

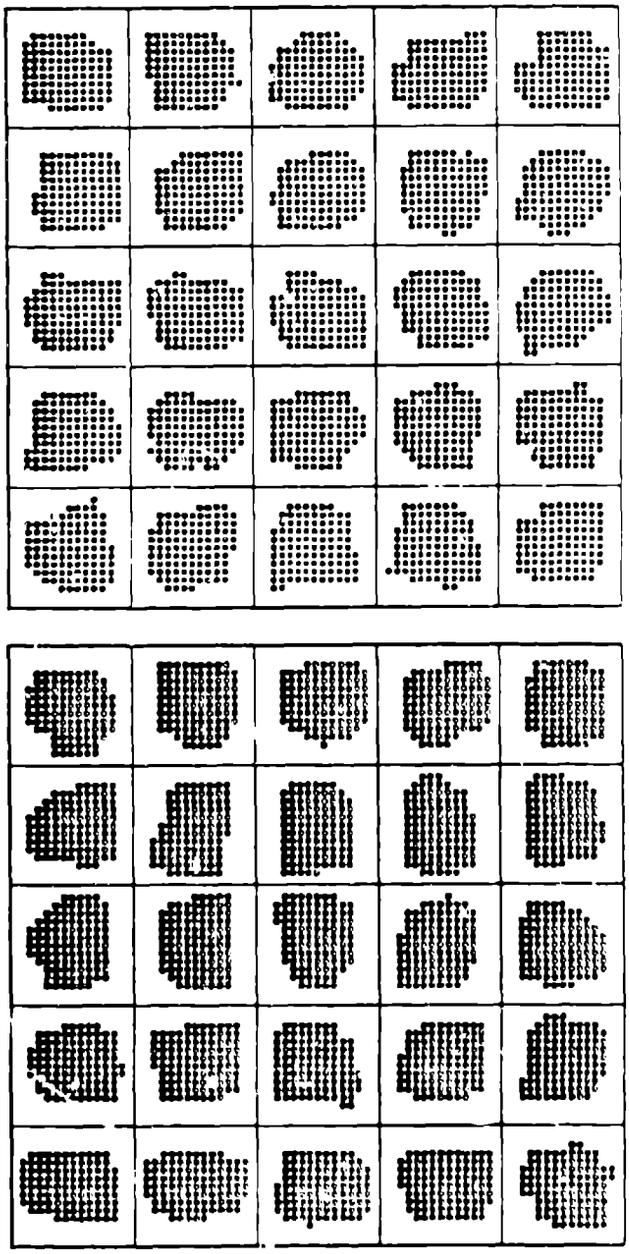

Fig. 9. Equal time shapshots of an n=100 adatom cluster (top) and an n=100 vacancy cluster (bottom) on Ag(100) at T=500K. The time between snapshots is 0.2 msec for both cases. Between successive snapshots the adatom cluster made ~300,000 steps and the vacancy cluster made ~95,000 steps.

Another interesting feature is that a passing monomer can act as a sort of catalyst to enhance the diffusion of a small block cluster. For example, below room temperature, an n=4 cluster is virtually immobile compared to an n=5 cluster. Thus, when the n=4 cluster absorbs a monomer, it suddenly starts to actively diffuse. When it later ejects a monomer, it becomes immobile again.

5. CONCLUSIONS

The overlayer dynamics method, in conjunction with an embedded atom-style potential, has been applied to the classical dynamics of clusters of Ag adatoms and vacancies on the Ag(100) surface. The adatom cluster diffusion is qualitatively similar to the diffusion observed for Lennard-Jones clusters on fcc(100).[10] Monomers diffuse the fastest, with E_A=11.3 kcal/mol. Larger clusters diffuse more slowly, though the decrease is not monotonic, because some small clusters can form stable blocks with high activation barriers to diffusion. The rate determining step for diffusion of large clusters is the 19.2 kcal/mole barrier for an adatom to climb onto a fresh edge from a kink site.

Vacancy clusters were also examined, and show the same features as adatom clusters, though they dissociate more rapidly (by ejection of a monomer), and nonproductive edge-running is less prevalent. A vacancy monomer diffuses faster (E_A = 10.7 kcal/mol) than an adatom on the Ag(100) surface, and is expected to contribute to mass transport with an activation energy of 22.6 kcal/mol, whereas the mass transport barrier for adatom diffusion is 26.1 kcal/mol.

From an estimate of the cluster dissociation lifetime, it appears that clusters at T=500K migrate between 1Å and 10 Å before dissociation (clusters

much larger than 100 atoms survive for a shorter distance), and vacancies survive for about 0.1 Å to 1 Å.

The treatment of some types of thin film growth with this method should be possible, by incorporating adsorption, desorption and multi-layer adatom jumps into the catalog.

REFERENCES

1. R.W. Vook, Int. Met. Rev. 27, 209 (1982).
2. J.A. Venables and G.D.T. Spiller, in Surface Mobilities on Solid Materials, edited by V.T. Binh, Vol. 86, (Plenum, New York, 1983), p. 341.
3. J.D. Weeks and G.H. Gilmer, Adv. Chem, Phys, 40, 157 (1979).
4. G.H.J. Gilmer and J.Q. Broughton, J. Vac. Sci. Tech. B 1, 298 (1983).
5. F.F. Abraham and G.M. White J. Appl. Phys. 41, 1841 (1970).
6. B. Liao and H.A. Macleod, Proc. SPIE-Int, Soc. Opt. Eng. 540, 150 (1985).
7. K.H. Müller, Appl. Phys.A, 40, 209 (1986).
8. J. Salik, J. Appl Phys. 57, 5017 (1985).
9. M. Schneider, A. Rahman, and I.K. Schuller, Phys. Rev. 34, 1802 (1986).
10. A.F. Voter, Phys. Rev. B. 34, 6819 (1986).
11. M.S. Daw and M.I. Baskes, Phys. Rev. B 29, 6443 (1984).
12. M.W. Finnis and J.E. Sinclair, Phil Mag. A 50, 45 (1984).
13. M. Manninen, Phys. Rev. B 34, 8486 (1986).
14. S.M. Foiles, M.I. Baskes, and M.S. Daw, Phys. Rev. B 33, 7983 (1986), and references therein.
15. Using the Lennard-Jones parameters from T. Halichioglu and G.M. Pound, Phys. Status Solidi A 30, 619 (1975), and along with the melting temperature of a Lennard-Jones crystal, which is 0.7ε.
16. W.A. Harrison, Pseudopotentials in the Theory of Metals (Benjamin, New York, 1966).
17. J.K. Norskov and N.D. Lang, Phys. Rev. B 21, 2131 (1980).
18. M.J. Stott and E. Zaremba, Phys. Rev. B 22, 1564 (1980).
19. M.J. Puska, R.M. Nieminen and M. Manninen, Phys. Rev. B 24, 3037 (1981).
20. J.K. Norskov, Phys. Rev. B 26, 2875 (1982).
21. A.F. Voter, to be published.
22. A.F. Voter and S.P. Chen, Proceedings of the Materials Research Society, Boston, Winter 1986, Symposium I (MRS Volume 82).
23. Equation (4) is the electron density for a 4s Slater orbital, appropriate for a first-row transition metal. This was found to work well for the six fcc metals fit in Ref. 21.
24. S.M. Foiles, Phys. Rev. B 32, 7685 (1985).
25. J.H. Rose, J.R. Smith, F. Guinea and J. Ferrante, Phys. Rev. B 29, 2963 (1984).
26. J.A. Nelder and R. Mead, Comp. J. 7, 308 (1965).
27. C. Kittel, "Introduction to Solid State Physics," 5th edition (Wiley, New York, 1976), p. 31.
28. Metal Reference Book, 5th ed., edited by C.J. Smith (Butterworths, London 19876), p. 186.
29. G. Simmons and H. Wang, Single Crystal Elastic Constants and Calculated Aggregate Properties: A Handbook (MIT Press, Cambridge, 1971).
30. R.W. Balluffi, J. Nucl. Mater. 69 & 70 240 (1978).
31. K.P. Huber and G. Herzberg, Constants of Diatomic Molecules (Van Nostrand Reinhold, New York, 1979), p. 8.
32. R_e for Ag_2 was estimated by scaling R_e for Cu_2 (Ref. 31, p. 198) using the fcc lattice constants for Cu and Ag from Ref. 23.
33. S. Glasstone, K.J. Laidler and H. Eyring, The Theory of Rate Processes (McGraw Hill, New York 1941).
34. J.D. Doll, J. Chem. Phys. 73, 2760 (1980); 74, 1074 (1981).
35. A.F. Voter and J.D. Doll, J. Chem. Phys. 80, 5832 (1984).
36. A.F. Voter, J. Chem. Phys. 82, 1890 (1985).
37. A.F. Voter and J.D. Doll, J. Chem. Phys. 82, 80 (1985).
38. D. Chandler, J. Chem. Phys. 68, 2959 (1978).
39. J.D. Doll and A.F. Voter, Ann. Rev. Phys. Chem. 38, 413 (1987).
40. J.C. Tully, G.H. Gilmer and M. Shugard, J. Chem. Phys. 71, 1630 (1979).
41. J.A. Panitz, J. Phys. E 15, 1281 (1982).